Journal Name

Nanostructure of solid electrolyte interphases and its consequences for microsized Sn anodes in sodium ion battery

Received 00th January 20xx,
Accepted 00th January 20xx

DOI: 10.1039/x0xx00000x

www.rsc.org/

Jiaqiang Huang,[a,#] Xuyun Guo,[a,#] Xiaoqiong Du,[a] Xiuyi Lin,[a] Jianqiu Huang,[a] Hong Tan,[a,b] Ye Zhu[a,*] and Biao Zhang[a,b,*]

There has been increasing evidence that ether-based electrolytes offer more stable battery performance, even for microsized alloy electrodes which suffer huge volume change upon charging/discharging cycling. It is speculated that ether-based electrolytes may give rise to more robust solid electrolyte interphases (SEIs), but the detailed mechanism remains unknown, due to the structural complexity and the extremely vulnerable nature of SEIs. In this work, we unveil the characteristic SEI structure at Sn electrode surfaces in both ester- and ether-based electrolytes. We adopt cryogenic transmission electron microscopy to probe the pristine SEI structure, in combination with X-ray photoelectron spectroscopy and density functional theory calculation. An ultrathin SEI forms in the ether-based electrolyte, with amorphous particles dispersed in polymer-like matrix. This unique nanostructure exhibits superior mechanical elasticity and renders anomalous stability against the large volume change of alloy electrodes, as evidenced by both electrochemistry measurement and atomic force microscopy. Our work demonstrates the potential of such an optimized SEI to enable the application of high-capacity anodes such as microsized alloys for alkali-metal ion batteries.

Metal ion batteries are one of the top choices for energy storage.[1] In pursuit of improved energy densities of batteries, high-capacity anode materials are preferred. However, a dramatic volume change occurs accompanying with the massive amount of ion insertions/desertions, particularly when the ion radius is large. As a result, the pulverization of electrodes and their loss of electrical contact take place,[2] when the diffusion-induced stress is huge enough for the crack nucleation/propagation.[3] The increasingly depleted active materials lead to the capacity decay. In addition, solid electrolyte interphase (SEI) is also susceptible to the volume change.[4, 5] The breakage of SEI deteriorates the Coulombic efficiencies, and its accumulation aggravates the ion transports.[4]

Nanostructured alloys have been utilized owing to their better resistance to fracture.[3, 6] Nevertheless, the production of nanomaterials is costly and hardly scalable due to the complicated synthesis.[2, 5] Furthermore, the large surface area of nanomaterials may give rise to low Coulombic efficiencies owing to the excessive formation of SEI.[5] Instead, the applications of microparticle materials have become feasible by self-healing polymers and highly elastic binders, which prevent the electrical disconnection after the pulverization.[2, 7] In view of SEI, coatings such as carbon,[4] graphene[5], and SiO_x[8] have been explored to eliminate the newly exposed interfaces. The coatings simultaneously confine the broken particles.[4, 5, 8] These studies provide invaluable insights into controlling the over-growth of SEIs to avoid the adverse effect. An intriguing question is whether the SEIs themselves, with optimized composition and structures, could also be favorable to cyclic stability.

SEI results from the energy mismatch between the reduction/oxidation potentials of electrolyte and the work functions of the electrode.[9] In aprotic electrolytes, the formation of SEI is inevitable for many electrodes including graphite, Si, and Sn. Among various electrolyte formulae, carbonates are the conventional solvents in most metal ion batteries, while ethers have drawn more attention in new systems including lithium-sulfur and metal anode batteries.[10-15] The anodic stability of ether is the major concern for matching with high-voltage cathodes. Fortunately, it is not an unsurmountable issue as demonstrated in the recent study.[16] Ethers have also demonstrated the remarkable capability to stabilize microparticle anodes including Sn and Bi for sodium and potassium ion batteries.[17-19] It is speculated the stabilization mechanism lies in the formation of dense SEIs which constrain the volume change. Despite these advances, the nanostructures and mechanical properties of electrolyte-derived SEIs remain largely unknown, which are essential to developing a general approach to stabilizing the microsized

[a]*Department of Applied Physics, The Hong Kong Polytechnic University, Hung Hom, Hong Kong, P.R. China*
[b]*The Hong Kong Polytechnic University Shenzhen Research Institute, Shenzhen, P.R. China*
#: These authors contribute equally to this work.
*Email: Dr. Biao Zhang: biao.ap.zhang@polyu.edu.hk; Dr. Ye Zhu: ye.ap.zhu@polyu.edu.hk
Electronic Supplementary Information (ESI) available: [Experimental and theoretical sections, Fig. S1-S26, Eq. S1-S43, and Movies 1 and 2]. See DOI: 10.1039/x0xx00000x

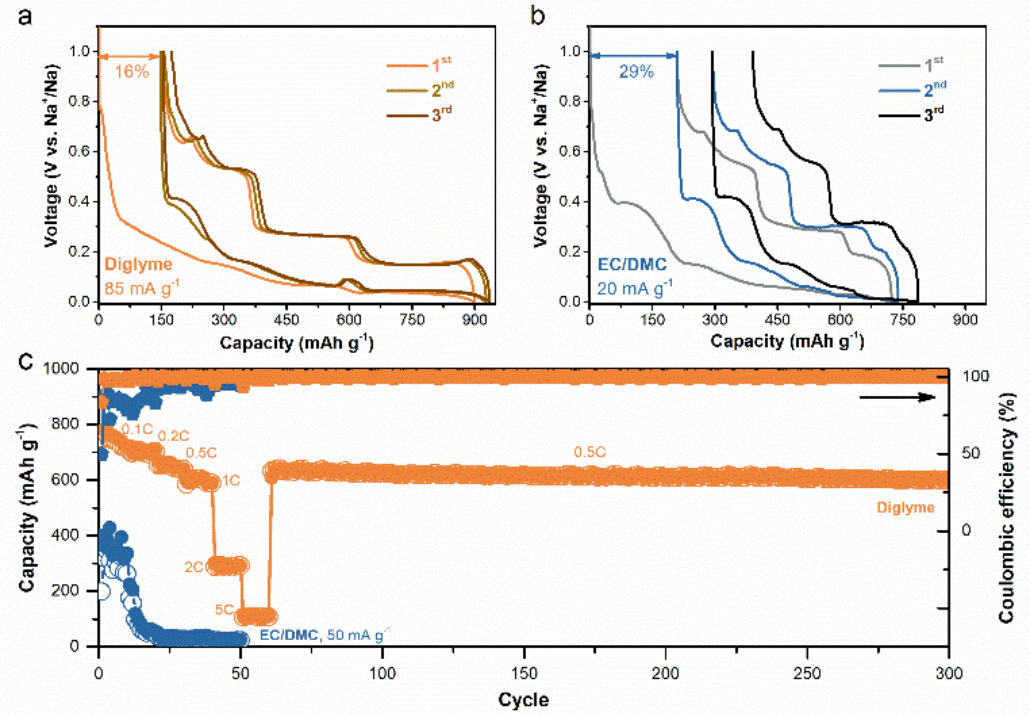

Fig. 1 Electrochemical behaviours. (a,b) The first three discharge/charge curves and (c) the cyclic stability of Sn microparticle electrodes in 1M $NaBF_4$/diglyme (a: 85 mA g^{-1}, c orange: rate test) and 1M $NaBF_4$/EC/DMC (b: 20 mA g^{-1}, c blue: 50 mA g^{-1}) electrolytes using the configuration of Na/Sn half cell.

alloy anodes through interphase engineering. In this work, using microparticle Sn in sodium ion batteries as a model system, we reveal the properties of two representative SEIs derived from carbonate and ether electrolytes. To overcome the vulnerable nature of SEIs, we utilize cryogenic transmission electron microscopy (cryo-TEM) and electron energy loss spectroscopy (cryo-EELS) to examine their pristine morphology and composition with inhibited beam damage. The corresponding mechanical properties including elasticity and stiffness are quantitatively measured using atomic force microscopy (AFM). The characteristics of an "ideal" SEI are therefore elucidated, which opens the avenue to stabilize microparticle anodes against the enormous volume expansion.

The superior stability of a Sn microparticle electrode (Fig. S1) in the ether-based electrolyte ($NaBF_4$/diglyme) is demonstrated in Fig. 1 and S2. Diglyme was selected instead of glyme or tetraglyme, considering the overall stability and ionic conductivity (Fig. S3).[20, 21] Compared to the $NaBF_4$/ethylene carbonate (EC)/dimethyl carbonate (DMC) electrolyte (Fig. 1b), the diglyme electrolyte delivers significantly improved Coulombic efficiencies (Fig. 1a), rate capabilities and cyclic stability (Fig. 1c). Similar electrochemical behaviors are seen (Fig. S3) whether using $NaPF_6$ as the salt or in the full-cell configuration (with $Na_3V_2(PO_4)_3$ to exclude the reactivity of sodium). The enhancement of rate capability in diglyme is surprising since the ionic conductivity of EC/DMC-based electrolyte is nearly two times that of diglyme.[22] The electrochemical stability in diglyme is also extraordinary considering the volume expansion of Sn is up to 430% and the diffusion-induced stress is magnified in the microparticle form compared to nanoparticles.[3, 17] An interesting hint from the electrochemical results is the readily high Coulombic efficiencies (>99% after 4th cycle) in diglyme, indicating the negligible formation of new SEI after the repeated volume change. In contrast, the irreversible capacity continuously accumulated (Fig. 1b,c) in carbonates as a sign of continuous electrolyte decompositions and new SEI formations. It further motivates the detailed investigations into the structures and properties of these two SEIs.[21]

Prior to experimental characterization, the bond-dissociation energy of the carbonate and diglyme molecules are theoretically examined via density functional theory (DFT) calculations to better understand the decompositions of these solvents and their contributions to SEIs (Fig. 2).[23-26] Bond-dissociation energy measures the strength of chemical bonds

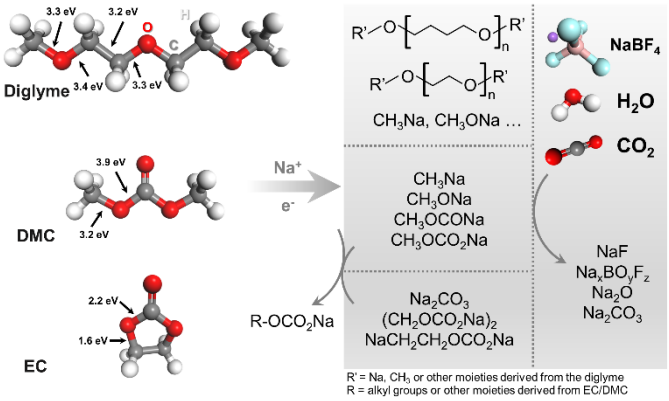

Fig. 2 Theoretical calculations. The molecular structures of EC, DMC, and diglyme together with the predicted decomposition products. The labile bonds are marked by arrows with the corresponding dissociation energies. The influences of $NaBF_4$, H_2O, and CO_2 are also considered, see the detailed homolysis (Fig. S4-S6) and the proposed reduction mechanisms (Eq. S1-S22).

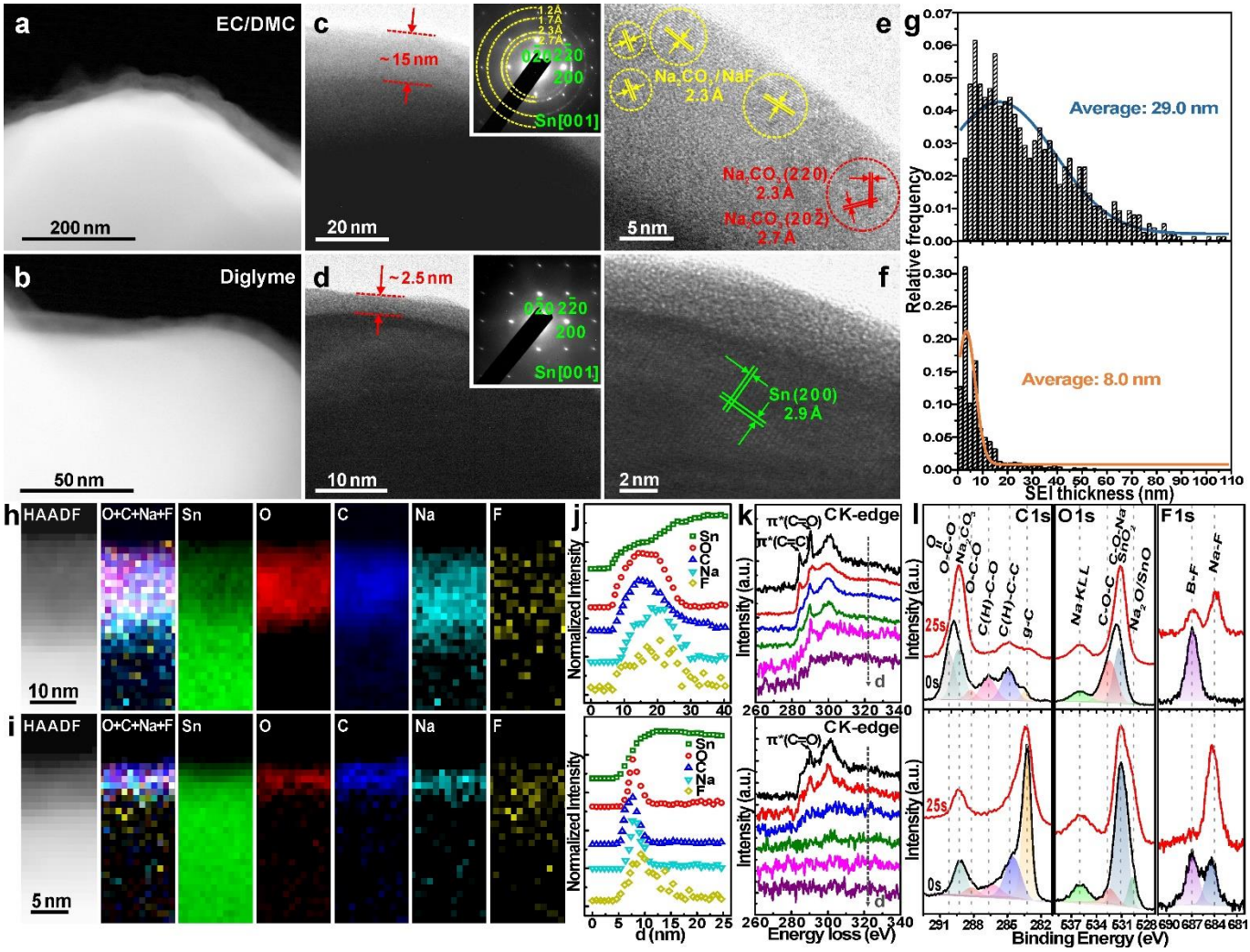

Fig. 3 Composition/nanostructure of SEIs probed by cryo-TEM and XPS. (a-f) High-angle annular dark field (HAADF) STEM and TEM images of SEIs in (a,c,e) $NaBF_4$/EC/DMC and (b,d,f) $NaBF_4$/diglyme with SAED as insets in (c,d). (g) Histograms showing the distributions of SEI thickness in $NaBF_4$/EC/DMC (top) and $NaBF_4$/diglyme (down) with >700 spots for each. (h-k) HAADF-STEM image, EELS mapping with the 1D averaged composition profiles, and high-resolution EELS spectra of SEIs in $NaBF_4$/EC/DMC (h, j and k top) and $NaBF_4$/diglyme (i, j and k down). Note that "d" in j and k denotes the position from vacuum to the Sn particles. (l) In-depth XPS spectra of C 1s, O 1s and F 1s of SEIs in $NaBF_4$/EC/DMC (top) and $NaBF_4$/diglyme (down). Argon sputtering was applied to acquire the depth profiles.

and suggests the possible radicals formed by homolysis. Apart from the C-H bonds, the C-O and C-C bonds of diglyme are both labile (Fig. 2 and S4). $NaBF_4$ tends to decompose into NaF and BF_3 (Eq. S1). The generated Lewis acids (BF_3 or PF_5 from $NaPF_6$) interact with the basic oxygen atoms in diglyme and thus strain the C-O bonds.[27] This enhances the C-O bond cleavages and renders radicals that are rich in $-OCH_2CH_2-$ for the oligo-/polymerization of polymer-like species (see Eq. S2-S7).[27] Such catalysts and the resultant polymer-like species may be the key to the improved electrochemical stability from the diglyme electrolyte: replacing $NaBF_4$ or $NaPF_6$ with other salts including $NaClO_4$, $NaSO_3CF_3$, and NaTFSI leads to deteriorated electrochemical performance (Fig. S7). Note that the formation of polymer-like species was widely reported in different ethers.[28, 29] Similarly, the C-O bonds are labile in DMC and EC (Fig. 2, S5, and S6). The decomposition of EC/DMC thus gives rise to methyl, methoxy and ester radicals. They further recombine with each other or sodium to form carbonate ester and inorganic carbonate (Eq. S8-S12).[28] In conjunction with the above radicals, the salt ($NaBF_4$) and inevitable contaminants (H_2O/CO_2) may generate NaF, $Na_xBO_yF_z$, Na_2O, and inorganic carbonates in both SEIs as shown in Eq. S13-S22.[28, 30] In addition, we suspect that binders may serve as a part of SEIs (Fig. S8). Overall, it is theoretically predicted that the decisive SEI components in diglyme and EC/DMC are polymer-like species and inorganic/organic carbonates, respectively. The lowest unoccupied molecular orbital (LUMO) and highest occupied molecular orbital (HOMO) were also calculated (Fig. S9). Despite the possible inaccuracy,[9] the relatively low LUMO of EC may contribute more to the reduction.

We adopt the recently developed strategy of using cryo-TEM to analyze the susceptible nanostructure of the SEIs without beam damage.[31-34] Prior to the observations, the batteries were cycled three times to form SEIs. Both TEM and scanning TEM (STEM) images (Fig. 3a-g) show much thicker SEI formed in EC/DMC than the diglyme one (29 vs. 8 nm on average). Interestingly, the selected area electron diffraction (SAED) pattern (Fig. 3c, inset) indicates the formation of polycrystalline components in EC/DMC-derived SEI. Those characteristic d-spacings may correspond to Na_2CO_3 (2.7, 2.3,

1.7 and 1.2 Å) and NaF (2.3 and 1.6 Å). The crossed lattice fringes (2.7 and 2.3 Å, 76°) in the high-resolution TEM (HRTEM) image (Fig. 3e, red) unambiguously confirm the presence of Na_2CO_3 nanocrystals (ICSD #95548), while those with a spacing of 2.3 Å can be ascribed to Na_2CO_3 or NaF. In contrast, the diglyme-derived SEI is poorly crystalline or amorphous, as indicated by both the SAED pattern (Fig. 3d, inset) and HRTEM image (Fig. 3f), possibly because the small thickness limits the nucleation and growth of crystals. Cryo-EELS was used to map the elemental distributions at nanoscale (Fig. 3h,i). Unexpectedly, Sn is identified in both SEIs, possibly in the form of SnO_x or organosiloxane-like species. Roughly, all elements including C, O, Na, and F are uniformly distributed in both SEIs, with C and O distributed slightly towards the surface compared to Na and F. This trend is more clearly observed in the 1D averaged composition profile in Fig. 3j. In addition, the fine structures in EELS (Fig. 3k) detect the surface-rich signals of C=C bonds in EC/DMC-derived SEIs, possibly indicating the adsorptions of ethylene (Eq. S10 and S12).[33] However, this signal is imperceptible in diglyme-derived SEIs. The C=O bonds in both SEIs verify the presence of carbonates as discussed. We emphasize that due to the extreme sensitivity of SEIs, the above TEM observation cannot be performed at room temperature without beam damage (Movies 1 and 2 for without and with cryo, respectively), demonstrating the power of cryo-TEM on characterizing susceptible nanostructure of SEIs. Note that replacing $NaBF_4$ with $NaPF_6$ does not change the nanostructures of SEIs (Fig. S10). In addition, the electrodeposited Sn was prepared to exclude the influences of additives on the characterizations (Fig. S11). Similar nanostructures were observed in the cycled, electrodeposited Sn electrodes (Fig. S12).

To further figure out the chemical species in SEIs, in-depth X-ray photoelectron spectroscopy (XPS) was applied (Fig. 3l). Organic carbonates (~290 eV) are formed in the EC/DMC-derived SEI but absent in the diglyme one. This is also verified by the one in electrodeposited Sn (Fig. S13). The fractions of C-C-O bond are 24% and 18% in glyme and EC/DMC, respectively. Considerable parts of O-C-O, C(H)-C-O and C(H)-C-C are from organic carbonates in EC/DMC-derived SEI but correspond to polymer-like species in the diglyme one.[35] Aside from C-C, C-C-O and organic carbonates are the major components for the

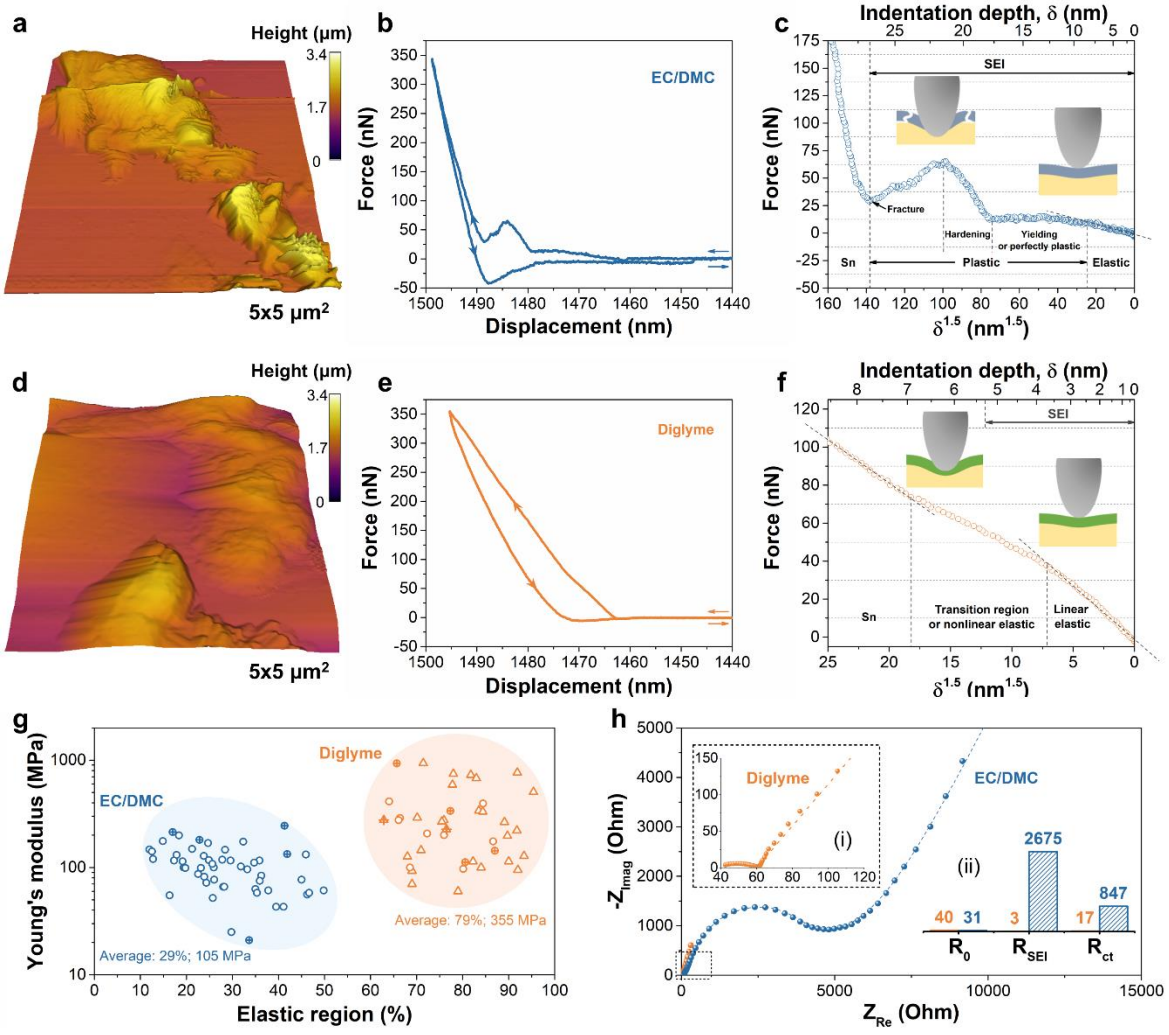

Fig. 4 Mechanical and ionic transport properties of SEIs. (a-f) AFM images, representative force spectroscopies and their detailed analysis of SEIs in (a-c) $NaBF_4$/EC/DMC and (d-f) $NaBF_4$/diglyme with schematics as insets in (c,f). (g) Distributions of Young's modulus and elastic regions of the SEIs with >30 curves for each. The responses with and without fracture/yielding behaviors are plotted by circle and triangle scatters, respectively. The results from electrodeposited Sn without binders and carbons are marked by additional "+". (h) Three-electrode EIS result of the cycled electrodes with (i) enlarged Nyquist plot in diglyme and (ii) the fitted impedance as the insets.

SEIs in diglyme and EC/DMC, respectively. The formation of polymer-like species is further supported by Raman spectroscopy (Fig. S14).[36] Na_2CO_3 and NaF are the main and minor inorganic components in both SEIs, respectively (Fig. 3l, S13c, and S15a). Other possible minor components in both SEIs include Na_2O, $Na_xBO_yF_z$, and Sn-containing species. The chemical compositions unraveled by XPS are largely consistent with the theoretical predictions (Fig. 2). The in-depth analysis further reveals that organic carbonates are surface-rich in EC/DMC-derived SEI as evidenced by the peak shifts in C 1s (~289.5 eV) and O 1s (~531.5 eV). Instead, NaF shows a surface-poor characteristic, consistent with the distribution observed in above Cryo-TEM elemental mapping. The depth profile cannot be seen by XPS in diglyme-derived SEI due to its small thickness versus the probing depth of XPS (Fig. S13b and S15b).

Based on the observations above, the EC/DMC-derived SEI is much thicker with crystalline domains of Na_2CO_3 (and possible NaF) embedded in organic carbonates and other amorphous phases. In contrast, the diglyme-derived SEI is ultrathin with amorphous particles such as Na_2CO_3/NaF dispersed in the polymer-like matrix.

The mechanical and ionic transport properties of SEIs directly impact the electrochemical behaviors of high-capacity anodes. Consequently, AFM was used to study their nanomechanics (Fig. 4a-g). According to Derjaguin, Muller, and Toporov (DMT) model,[37, 38]

$$P - P_{c,DMT} = \frac{4E_1\sqrt{R_2}}{3(1-\nu_1^2)}\delta^{1.5} \quad (1)$$

where P is the indenter load, $P_{c,DMT}$ is the pull-off force, E_1 is the Young's modulus of the sample, R_2 is the indenter radius, ν_1 is the Poisson's ratio of the sample, and δ is the indentation depth. See derivation in Eq. S23-S30. Eq. 1 enables the determination of linear elastic region. After imaging (Fig. 4a,d and S15), the force spectroscopies on microsized particles were collected (Fig. 4b,e). The EC/DMC-derived SEI shows distinguishable force responses at different stages (Fig. 4c), including (i) a linear elastic region; (ii) a quasi-constant-force region, indicating a yielding or perfectly plastic process; (iii) a non-linear force increase, suggesting a hardening process; (iv) a force decrease as a sign of SEI and/or interfacial fractures. In contrast, the representative force responses of the diglyme-derived SEI (Fig. 4f) resemble the behavior of elastomers, consisting of (i) a linear elastic region; (ii) a slope change indicating the response from Sn or the non-linear elastic part. Fracture behavior was also found in diglyme-derived SEI (Fig. S16) at some spots (Fig. 4g, orange circle). We examine the stiffness and elasticity of the SEIs, which are correlated to their mechanical stability against the volume expansion. To further quantify their difference, the Young's modulus, the elastic region, and the thickness were calculated, see Fig. 4g, S17, and S18. The diglyme-derived SEI is stiffer (~355 MPa) and more elastic (~79%) than its EC/DMC counterpart (~105 MPa, ~29%), and the SEI thickness obtained by AFM (Fig. S19c) is consistent with the observations via cryo-TEM. In addition, the AFM results of electrodeposited Sn, which exclude the complexity from carbons/binders, also support the above discussions (Fig. S20 and 4g, "+"-marked points). To quantitively correlate the elastic region with the electrochemical behaviors, the strain of SEI upon the volume expansion is derived, see Eq. S31-S43 and Fig. S21-S23. Fig. S24a shows that the EC/DMC-derived SEI only sustains a relatively low capacity ranging from 151 to 515 mAh g^{-1} without the irreversible plastic deformation. Its mechanical property can be further deteriorated due to the SEI inhomogeneity as discussed above (Fig. 3). On contrary, the diglyme-derived SEI is theoretically tolerant to the volume expansion upon the full sodiation (Fig. S24), despite the possible overestimation arising from the homogeneity approximation. Note that simplifications in the AFM analysis and model give rise to some quantitative inaccuracy without detrimental to the final conclusions. Aside from the mechanics, the ionic transport properties of the SEIs were characterized by electrochemical impedance spectroscopy (EIS), which identifies the local resistance by frequencies (Fig. 4h). Quantified with an equivalent circuit (Fig. S25),[39] the three-electrode EIS results suggest that the resistances arising from the SEI (R_{SEI}) and the SEI/electrolyte interface (R_{ct}) in diglyme are 2-3 orders of magnitude lower than the EC/DMC ones. The galvanostatic intermittent titration technique (GITT) results also validate this (Fig. S26),[40] showing that the apparent diffusivities in diglyme are higher than the one in EC/DMC by 2-3 orders of magnitude.

Resolving the origins of properties (Fig. 1 and 4) from the composition/structure (Fig. 3) of SEIs is essential for the rational design of SEIs. (i) The elastic properties. The superior elasticity of SEI explains the exceptional electrochemical stability in diglyme (Scheme 1). From the composite point of view, the matrix and filler are equally important. While polymer-like species maybe be elastic,[28] the carbonate ester without long molecular chains is likely plastic. As for the fillers, the ionic bonds of crystalline domains (Na_2CO_3/NaF) in EC/DMC-derived SEI restrict the slip or motion of dislocations, leading to their brittle nature. On the contrary, the amorphization of particles in diglyme-derived SEI facilitates the breaking and reforming of interatomic bonds. Despite the unknown matrix-particle interactions, elastic matrix and amorphous particle are preferred for better elasticity towards the huge volume expansion. (ii) The ionic transport properties. The magnified ionic conductivity through the SEI and SEI/particle interface clarifies the surprising rate capability in diglyme (Scheme 1). Diffusion length and diffusivity are both fundamentally vital. Apparently, the reduced thickness of diglyme-derived SEI largely decreases the sodium diffusion length through the SEI. In addition, crystalline Na_2CO_3 and NaF deliver poor sodium diffusivities of ~6×10^{-34} and ~2×10^{-49} cm^2 s^{-1}, respectively.[41] However, their ionic conductivity is very likely enhanced via the amorphization, similar to the case of Li_2O_2 (by 12 orders of magnitude).[42] This further explains the improved transport properties of diglyme-derived SEI.

The desired merits for an ideal SEI of high-capacity anodes are further discussed (Scheme 1). (i) Thin. This feature is

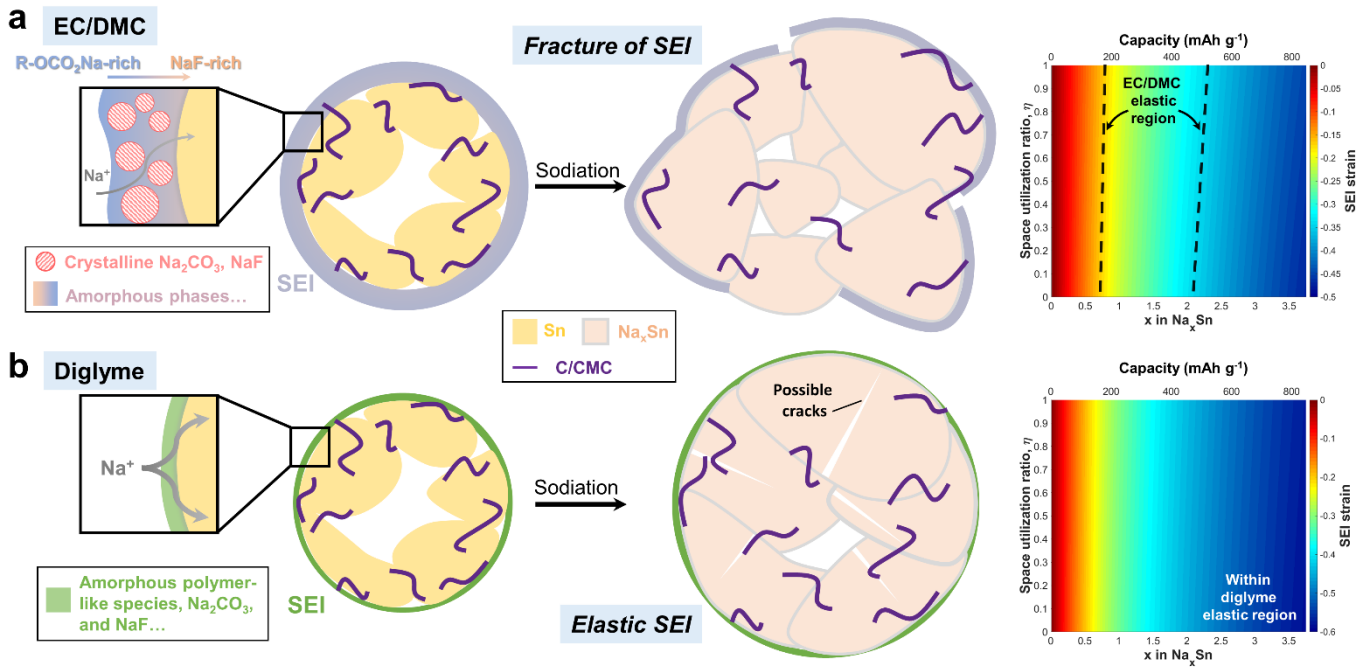

Scheme 1. Schematics illustrating the chemical compositions, structures and the mechanical response to the volume expansion of SEIs derived from (a) $NaBF_4$/EC/DMC and (b) $NaBF_4$/diglyme. The strains imposed on the SEI as a function of *x* in Na_xSn and space utilization ratio in comparison to the elastic region of SEIs are also included.

particularly favorable for the ionic transport and may suppress the nucleation and growth of crystalline particles for better elasticity. In addition, it implies the suppressed reduction of electrolytes and namely high Coulombic efficiencies. This demanding merit requires smart selections of electrolyte or fabrication of artificial SEI. (ii) Elastic. SEIs are expected to reversibly, elastically deform under the huge volume expansion without irreversible plastic deformation and fractures. It necessitates the formation (or artificial inclusion) of superior elastomers. (iii) A high ionic diffusivity. As discussed, this may be enhanced by the amorphization of embedded particles. (iv) A reasonably high stiffness. The optimal stiffness of SEI remains an open question.[43] However, a higher stiffness may help to prevent the (broken) particles from electrical disconnection upon the anisotropic volume expansion (Scheme 1). The modulus of composite SEI is closely correlated to the ones of matrix and fillers according to the rule of mixtures.

In summary, the structure/composition and properties of EC/DMC- and diglyme-derived SEIs have been unraveled. Though thin, the diglyme-derived SEI delivers high elasticity and ionic conductivity, due possibly to the special structure with amorphous particles dispersed in polymer-like species. On the contrary, the composite SEI consisting of crystalline domains and carbonate ester delivers poor mechanical and transport behaviors. These results will provide important implications in the quest for the rational design of electrolyte/electrode interphases.

Conflicts of interest

There are no conflicts to declare.

Author Contributions

B.Z. conceived the idea and supervised the whole project. J. H. conducted the theoretical calculations, electrochemical tests, and analysis. X. G. and Y.Z performed the TEM characterizations. B.Z., J.H., X.G., and Y.Z. wrote the manuscript and all authors discussed the experiments and final manuscript.

Acknowledgements

The authors are grateful to Prof. Jean-Marie Tarascon from College de France for critical reading of the manuscript. This work was financially supported by the Hong Kong Polytechnic University (Grant 1-ZE83), the Innovation and Technology Commission (ITF Project ITS/029/17) of Hong Kong SAR, and the Key Project for Basic Research of Shenzhen (No. JCYJ20170818104125570). S/TEM work was carried out at the Hong Kong Polytechnic University and was supported by the Hong Kong Research Grants Council through the Early Career Scheme (Project No. 25301617) and the Hong Kong Polytechnic University grant (Project No. 1-ZE6G). Dr. X. G. and Dr. Y. Z. thank Dr. Wei Lu for optimizing the JEOL JEM-2100F microscope.

Notes and references

1. M. Armand and J.-M. Tarascon, *Nature*, 2008, **451**, 652.
2. C. Wang, H. Wu, Z. Chen, M. T. McDowell, Y. Cui and Z. Bao, *Nat. Chem.*, 2013, **5**, 1042-1048.
3. R. Deshpande, Y.-T. Cheng and M. W. Verbrugge, *J. Power Sources*, 2010, **195**, 5081-5088.
4. N. Liu, Z. Lu, J. Zhao, M. T. McDowell, H. W. Lee, W. Zhao and Y. Cui, *Nat. Nanotechnol.*, 2014, **9**, 187-192.
5. Y. Li, K. Yan, H.-W. Lee, Z. Lu, N. Liu and Y. Cui, *Nat. Energy*, 2016, **1**, 15029.

6. C. K. Chan, H. Peng, G. Liu, K. McIlwrath, X. F. Zhang, R. A. Huggins and Y. Cui, *Nat. Nanotechnol.*, 2008, **3**, 31-35.
7. S. Choi, T.-w. Kwon, A. Coskun and J. W. Choi, *Science*, 2017, **357**, 279-283.
8. H. Wu, G. Chan, J. W. Choi, I. Ryu, Y. Yao, M. T. McDowell, S. W. Lee, A. Jackson, Y. Yang, L. Hu and Y. Cui, *Nat. Nanotechnol.*, 2012, **7**, 310-315.
9. P. Peljo and H. H. Girault, *Energy Environ. Sci.*, 2018, **11**, 2306-2309.
10. S. Bai, X. Liu, K. Zhu, S. Wu and H. Zhou, *Nat. Energy*, 2016, **1**, 16094.
11. S. Jiao, X. Ren, R. Cao, M. H. Engelhard, Y. Liu, D. Hu, D. Mei, J. Zheng, W. Zhao, Q. Li, N. Liu, B. D. Adams, C. Ma, J. Liu, J.-G. Zhang and W. Xu, *Nat. Energy*, 2018, DOI: 10.1038/s41560-018-0199-8.
12. H. Kim, J. Hong, G. Yoon, H. Kim, K.-Y. Park, M.-S. Park, W.-S. Yoon and K. Kang, *Energy Environ. Sci.*, 2015, **8**, 2963-2969.
13. J. Zhang, D.-W. Wang, W. Lv, S. Zhang, Q. Liang, D. Zheng, F. Kang and Q.-H. Yang, *Energy Environ. Sci.*, 2017, **10**, 370-376.
14. M. Goktas, C. Bolli, E. J. Berg, P. Novák, K. Pollok, F. Langenhorst, M. v. Roeder, O. Lenchuk, D. Mollenhauer and P. Adelhelm, *Adv. Energy Mater.*, 2018, **8**, 1702724.
15. Z.-L. Xu, K. Lim, K.-Y. Park, G. Yoon, W. M. Seong and K. Kang, *Adv. Funct. Mater.*, 2018, **28**, 1802099.
16. S. Jiao, X. Ren, R. Cao, M. H. Engelhard, Y. Liu, D. Hu, D. Mei, J. Zheng, W. Zhao and Q. Li, *Nat. Energy*, 2018, **3**, 739.
17. B. Zhang, G. Rousse, D. Foix, R. Dugas, D. A. Corte and J. M. Tarascon, *Adv. Mater.*, 2016, **28**, 9824-9830.
18. C. Wang, L. Wang, F. Li, F. Cheng and J. Chen, *Adv. Mater.*, 2017, **29**, 1702212.
19. J. Huang, X. Lin, H. Tan and B. Zhang, *Adv. Energy Mater.*, 2018, **8**, 1703496.
20. L. Lutz, W. Yin, A. Grimaud, D. Alves Dalla Corte, M. Tang, L. Johnson, E. Azaceta, V. Sarou-Kanian, A. Naylor and S. Hamad, *J. Phys. Chem. C*, 2016, **120**, 20068-20076.
21. A. Ponrouch, E. Marchante, M. Courty, J.-M. Tarascon and M. R. Palacin, *Energy Environ. Sci.*, 2012, **5**, 8572-8583.
22. K. Westman, R. Dugas, P. Jankowski, W. Wieczorek, G. Gachot, M. Morcrette, E. Irisarri, A. Ponrouch, M. R. Palacín, J. M. Tarascon and P. Johansson, *ACS Appl. Energy Mater.*, 2018, **1**, 2671-2680.
23. P. E. Blöchl, *Phys. Rev. B: Condens. Matter Mater. Phys.*, 1994, **50**, 17953.
24. G. Kresse and J. Furthmüller, *Phys. Rev. B: Condens. Matter Mater. Phys.*, 1996, **54**, 11169.
25. J. P. Perdew, K. Burke and M. Ernzerhof, *Phys. Rev. Lett.*, 1996, **77**, 3865.
26. S. Grimme, *J. Comput. Chem.*, 2006, **27**, 1787-1799.
27. J. Dale, K. Daasvatn and T. Grønneberg, *Macromol. Chem. Phys.*, 1977, **178**, 873-879.
28. D. Aurbach, *J. Power Sources*, 2000, **89**, 206-218.
29. G. Zhuang and P. N. Ross Jr, *J. Power Sources*, 2000, **89**, 143-148.
30. K. Kanamura, H. Tamura and Z.-i. Takehara, *J. Electroanal. Chem.*, 1992, **333**, 127-142.
31. Y. Li, Y. Li, A. Pei, K. Yan, Y. Sun, C.-L. Wu, L.-M. Joubert, R. Chin, A. L. Koh and Y. Yu, *Science*, 2017, **358**, 506-510.
32. X. Wang, M. Zhang, J. Alvarado, S. Wang, M. Sina, B. Lu, J. Bouwer, W. Xu, J. Xiao, J. G. Zhang, J. Liu and Y. S. Meng, *Nano Lett.*, 2017, **17**, 7606-7612.
33. M. J. Zachman, Z. Tu, S. Choudhury, L. A. Archer and L. F. Kourkoutis, *Nature*, 2018, **560**, 345.
34. X. Wang, Y. Li and Y. S. Meng, *Joule*, 2018, **2**, 2225-2234.
35. R. Dedryvère, L. Gireaud, S. Grugeon, S. Laruelle, J.-M. Tarascon and D. Gonbeau, *J. Phys. Chem. B*, 2005, **109**, 15868-15875.
36. J. Koenig and A. Angood, *J. Polym. Sci. A*, 1970, **8**, 1787-1796.
37. B. V. Derjaguin, V. M. Muller and Y. P. Toporov, *J. Colloid Interface Sci.*, 1975, **53**, 314-326.
38. X. Shi and Y.-P. Zhao, *J. Adhes. Sci. Technol.*, 2004, **18**, 55-68.
39. M. Levi, G. Salitra, B. Markovsky, H. Teller, D. Aurbach, U. Heider and L. Heider, *J. Electrochem. Soc.*, 1999, **146**, 1279-1289.
40. C. J. Wen, B. Boukamp, R. A. Huggins and W. Weppner, *J. Electrochem. Soc.*, 1979, **126**, 2258-2266.
41. F. A. Soto, A. Marzouk, F. El-Mellouhi and P. B. Balbuena, *Chem. Mater.*, 2018, **30**, 3315-3322.
42. F. Tian, M. D. Radin and D. J. Siegel, *Chem. Mater.*, 2014, **26**, 2952-2959.
43. Y. Gu, W.-W. Wang, Y.-J. Li, Q.-H. Wu, S. Tang, J.-W. Yan, M.-S. Zheng, D.-Y. Wu, C.-H. Fan and W.-Q. Hu, *Nat. Commun.*, 2018, **9**, 1339.